Chapter 5

# High-Brightness Solid-State Lasers for Compact Short-Wavelength Sources

Akira Endo

Additional information is available at the end of the chapter

http://dx.doi.org/10.5772/64147

**Abstract**

Various types of compact short-wavelength sources are emerging in the region from EUV to hard X-ray and further to gamma ray. These high-energy photons are usually accessible in a large-scale facility such as SR or FEL, and the compactness of these new technologies provides new possibilities for broader applications in dedicated laboratories or factories. Laser-produced plasma is used for soft X-ray laser and high average power EUV sources for lithography. Laser Compton short-wavelength sources are now entering into practical applications in medical imaging. The performance of these sources critically depends on the laser driver performance. This chapter describes the recent progress of high-brightness, short-pulse solid-state laser technology in close relation to these new compact short-wavelength sources. Pulsed picosecond thin disc laser progress is reviewed with kW average power specifications. Cryogenic laser is reported for the advantage of higher beam quality in large-pulse energy operation.

**Keywords:** thin disc laser, cryogenic laser, plasma EUV source, laser Compton X-ray source

## 1. Introduction

A rapid progress is recently observed in the field of compact extreme-ultraviolet (EUV) and X-ray sources with high brightness and small footprint enough to be installed in laboratories in educational and research institutions, manufacturing facilities, hospitals, and other suitable sites [1]. This may advance scientific and technical disciplines in practical applications by complementing large-scale synchrotron radiation and free-electron laser sources. Applications span a wide range from biomedical, semiconductor, fundamental and applied

research, environmental engineering to industrial nondestructive testing. Component technology progress is one of the key factors in these advancements of the compact EUV through hard-X-ray sources. These key elements are instrumentation, optics, detectors, data management and processing, and one of the most significant factors is the progress of high average power, short-pulse solid-state lasers.

Semiconductor industry has been struggling in the past two decades to establish a technological system of extreme-ultraviolet lithography as the ultimate scheme, and the establishment of reliable, high average power (>100 W) 13.5 nm source has been always the most critical challenge. The basic architecture is now realized as the LPP (laser-produced plasma) EUV source, in which the conditioning of the mist target from a liquid tin droplet is essential for higher conversion efficiency and perfect recovery of the injected tin atoms [2]. The mist formation is performed by a diverging shock wave inside the microdroplet, which is driven by an impulse generated by an irradiation of picosecond solid-state laser pulse of mJ level pulse energy. The system repetition rate is typically 100 kHz, and the laser average power is more than 100W. The size of the droplet is 10 μm in diameter, and the required laser beam quality and stability must meet the requirements.

Lasing was reported in the EUV spectrum region by efficient excitation of dense plasma columns at 100 Hz repetition rate using a tailored pump pulse profile of a 1 J picosecond cryogenic Yb:YAG laser [3]. The average power of the 1 J picosecond laser is 100 W. The tabletop soft-X-ray laser average power is 0.1 mW at $\lambda$ = 13.9 nm and 20 μW at $\lambda$ = 11.9 nm from transitions of Ni-like Ag and Ni-like Sn, respectively. Lasing on several other transitions with wavelengths between 10.9 and 14.7 nm was also reported. The efficient X-ray laser operation was realized by an optimized pump pulse design as a nanosecond prepulse followed by two picosecond pulses to create higher density plasma of Ni-like ions of higher temperature for higher gain in longer time and in larger space. The high average power of these compact soft X-ray lasers promises to enable various applications requiring high photon flux with coherence.

Laser Compton X-ray source has been established as a compact, high-brightness short-wavelength source. The basic principle is similar to an undulator emission, and a high-intensity laser field is used as the modulating electromagnetic field. The laser Compton X-ray source is demonstrated as a compact short-wavelength imaging approach combined with the phase contrast method of biosamples. Single-shot imaging is critical for many practical applications, and the required specification depends on the usable laser pulse with some threshold parameters because all other component technologies are well matured. The optimization of the laser Compton hard X-ray source by single-shot base is already studied in detail [4, 5]. Experimental results well agreed with theoretical predictions. Highest peak brightness is obtained in the configuration of counterpropagating laser pulse and electron beam bunch, in the minimum focusing area before nonlinear threshold [6, 7]. A single-shot phase contrast bioimaging was demonstrated in the hard X-ray region [8]. The employed laser was a picosecond $CO_2$ laser of 3 J pulse energy [9], but the laser system was not an easy and compact one for further broad applications in various laboratories and hospitals. The Extreme Light Infrastructure–Nuclear Physics (ELI–NP) facility will have a brilliant $\gamma$-beam of $10^4$ photons/s/eV, ≤0.5% bandwidth,

http://dx.doi.org/10.5772/64147

with $E\gamma < 19.5$ MeV, which is obtained by the laser Compton method from an intense electron beam (Ee > 700 MeV) produced by a warm linac [10]. The main purpose is to provide an opportunity for the production of radioisotopes for medical research. The repetition rate is 100 Hz with a 1 J, picosecond Yb:YAG laser. A standard laser Compton X ray source is under construction as the STAR project at the University of Calabria (Italy) to generate monochromatic tunable, ps-long, polarized X-ray beams, ranging from 20 to 140 keV. The X-rays will be devoted to experiments of material science, cultural heritage, advanced radiological imaging with microtomography capabilities [11]. An S-band RF gun produces electron bunches at 100 Hz, boosted up to 60 MeV by a 3 m long S-band cavity. It is critical to use a high-brightness linac of low emittance and high pointing stability to focus higher charge bunch to a smaller spot size down to 10 μm. The allowed spatial stability is a few μm. The research and development of the X-ray generation laser is the key technology for higher and stable X-ray generation. The Yb:YAG laser is ideal for a compact, high pulse energy picosecond pulse and should be synchronized to the RF system in less than picosecond time jitter.

Compact short-wavelength sources are emerging due to the progress of extreme ultraviolet lithography (EUVL) in semiconductor industry. The EUVL has been intensively developed in the field of various component technologies, for example, Mo/Si high reflectivity mirror at 13.5 nm wavelength, new types of resist of higher sensitivity at this wavelength, and plasma-based 100 W class stable EUV sources. Further increase of average power is expected for large-scale manufacturing to kW level and shorter wavelength to 6.7 nm where a higher reflectivity mirror seems available. The necessity to evaluate an alternative approach is recently proposed based on high repetition rate free electron laser (FEL), to avoid a risk of the source power limit by the plasma-based technology. The possibility is indicated to realize a high repetition rate (superconducting) FEL to generate a multiple kW 13.5 nm light. It is important to note that the present FEL pulses are characterized typically as 0.1 mJ pulse energy, 100 fs pulse duration, and 1 mm beam diameter, and generated in the SASE mode. The beam fluence is higher than the ablation threshold of typical resists, and the beam has a higher spatial coherence, which leads to speckle patterns. The beam is composed of many short spikes with high peak intensities [12]. Seeding an FEL with an external coherent source has been studied together with SASE operation to increase the brightness and pointing/energy stability compared to SASE mode. An efficient seeding method was established by using UV wavelength laser in which the seed laser modulates the electron beam into coherent bunching at the harmonics of the seed laser wavelength. The bunching is intensified in another undulator for coherent FEL action, and the method is named as high-gain higher harmonic generation (HGHG). A successful demonstration is reported from FERMI as a double stage-seeded FEL with a fresh bunch injection technique [13]. The fresh bunch scheme was demonstrated as the FEL radiation produced by one HGHG stage acts as an external seed for a second HGHG stage. A 10 Hz demonstration was reported in the EUV wavelength region. The development of higher repetition rate FEL requires new optical laser developments to meet the needs of laser-induced FEL seeding. Conventional copper accelerating cavities operate up to tens to hundreds of hertz, but superconducting (SC) cavities, allow a much higher repetition rate of up to few megahertz. FLASH at DESY has a maximum repetition rate of 1 MHz within a burst structure (electron bunch train) of 800 μs at 10 Hz. Future linear accelerator designs plan an SC linear accelerator

capable of a continuous repetition rate of up to 1 MHz. This presents major challenges for the design and operation of laser-seeded FELs in both burst and continuous mode. At lower repetition rates, conventional Ti:Sapphire lasers are currently used for laser-induced FEL seeding at, for example, FERMI FEL-1. The future requirements of a tunable, high repetition rate laser with sufficient pulse energy can be met with optical parametric chirped-pulsed amplification (OPCPA). A tunable OPCPA is demonstrated at 112 W in burst mode. The center wavelength is located in the wavelength region of 720–900 nm. The repetition rate is 100 kHz and the pulse energy is 1.12 mJ with 30 fs pulse duration. The OPCPA pumping laser power limits the scalability of the OPCPA output, and it was demonstrated for a 6.7–13.7 kW (burst mode) thin-disk OPCPA-pump amplifier, increasing the possible OPCPA output power to many hundreds of watts. Furthermore, the third and fourth harmonic generation experiments are performed for the FEL seeding purpose [14].

Recent solid-state laser progress is closely related to the demands in the field of laser microablation in industry. Fiber laser is advancing in the high repetition rate, short-pulse operation mode in the subpicosecond pulse length. Significant progress has been made on the scaling of the performance of subpicosecond fiber laser systems in the past decade. The current limitation exists in the achievable peak power and average power of a linear amplifier. The maximum of the available average power in a single fiber laser is determined by the mode instabilities. Several hundred watts is the typical maximum power, depending on the properties of the fiber and other system parameters. The pulse energy is ultimately limited by the extractable energy of the fiber, nonlinear pulse distortions, and damage issues. Four coherently combined fiber amplifiers were reported as a single CPA system [15]. The average power was 530 W and combined pulse energy was 1.3 mJ. It is expected to realize higher system parameters from a beam combined fiber laser, especially in higher average power in pulsed mode. The beam quality was excellent and the beam combination efficiency was as high as 93%. It is expected that with the coherent combination concept and further progress in fiber laser technology, average powers in the range of 1 kW and pulse energy of 10 mJ are realistic parameters in the future. A 10 J, 10 kHz femtosecond laser system is under conceptual design by a coherent combination of 10,000 fibers as the extension of the coherent combining scheme for high repetition rate PW laser [16].

Another promising laser is the InnoSlab laser, which is a thin slab laser cooled from both surface and is reported as a Yb:YAG InnoSlab amplifier with femtosecond pulses of <3 mJ pulse energy with a repetition rate of 100 kHz. The chirped pulse amplification is essential to achieve high average power generation in the power amplifier stage. The laser system is consisted of a 10 mW seed laser with a pulse repetition rate of 100 kHz to MHz, and a preamplifier stage, and a high power InnoSlab amplifier which is followed by a grating pulse compressor. This laser system is ideal for OPCPA pumping and micromaterial processing [17]. The highest average power picosecond laser was reported from a thin-disk multipass laser amplifier, delivering 1.4 kW with pulses of 4.7 mJ pulse energy and duration of 8 ps at 300 kHz repetition rate [18]. The beam quality factor was better than M2 = 1.4. The experiments showed that the thin-disk multipass amplifier can scale pulse energy and average output power independently in the repetition rates between 300 and 800 kHz. Frequency doubling by means of an LBO

http://dx.doi.org/10.5772/64147

crystal led to 820 W of average power at a wavelength of 515 nm with 1170 W of incident IR power which corresponded to a conversion efficiency of 70% and an SHG pulse energy of 2.7 mJ. By sum-frequency generation between the beams at 1030 and 515 nm in a second LBO crystal, an average UV power of 234 W (780 μJ of pulse energy) was generated at the wavelength of 343 nm with a conversion efficiency of 32%. The output powers in the green and UV spectral region are limited by thermal effects and the apertures of the crystals employed. Future work may try to use shorter seed pulses as well as to increase the output power by implementing a higher number of passes in the amplifier and the pump module and by increasing the pump power. For the higher harmonic generation, crystals with larger apertures and an improved temperature control is critical to further improve the performance.

Carbon fiber-reinforced plastic (CFRP) is the most promising light material in aircraft or similar machines. CFRP was processed with the kW picosecond laser with 8 ps pulses and an average output power of up to 1.1 kW at a pulse repetition rate of 300 kHz with a maximum pulse energy of 3.7 mJ. Heat accumulation influences are studied for the processing quality in high average power operation [19]. The pulse overlapping and repetitive scans are studied for the heat accumulation effect in the report. The study indicates an estimation of optimized feed rates and maximum scan speeds. The kW picosecond thin disc laser demonstrated its applicability in the cutting application of a 2 mm CFRP with a high cutting speed of 0.9 m/min and smaller thermal damage less than 20 μm. These lasers, such as fiber, InnoSlab, and thin disc, have been proving solutions for high beam quality, short-pulse generation in the high average power regime in the past two decades. An alternative approach was reported by a cryogenically cooled Yb:YAG by demonstration to have significant potential for efficient near-diffraction-limited high average power lasers [20]. A single-pass amplifier was reported with 250 W output power, 54% optical-optical efficiency, M2= 1.1 and a power oscillator with 300 W output power demonstrated 64% optical-optical efficiency, and M2= 1.2. In each case, the laser systems were based on end-pumped laser rod gain modules cryogenically cooled in liquid nitrogen cryostats. The single-pass amplifier is a simple way, compared to fiber or thin disc, to boost the power of a laser oscillator. The output power in the experiments was limited only by the incident pump power. The cryogenically cooled, bulk Yb:YAG four-pass amplifier was operated at 100 kHz repetition rate [21]. The amplified optical pulses were 2.5 mJ pulse energy with <20 ps pulse length before compression and the spectrum for 3.6ps in transform limited duration. The measured power stability was less than 0.5% in half an hour full power operation. A flat-top spatial profile was measured with near-diffraction-limited beam divergence. This compact amplifier is ideal for pumping of OPCPA. This chapter describes recent progress of high average power, picosecond thin-disc laser from the research and development of the HiLASE project during 2012–2015. HiLASE R&D laser center is a technological infrastructure in Dolní Břežany near Prague in the Czech Republic, which was founded in a close connection to the ELI activity. Major effort is to develop lasers for high-tech application, in which the short-wavelength generation is one of the dominant ones. HiLASE focuses on the development of kW-class thin-disk-based picosecond and subpicosecond lasers from mJ to sub-1-J pulse energy. Laser pulses are emitted at repetition rates from 1 to 100 kHz with prospective upgrade up to 1 MHz near fundamental wavelength. In order to cover the broadest application potential

of the lasers, it was also initiated high-power harmonic frequency generation and high-power mid-IR picosecond system consisting of an OPG followed by double OPA systems (**Figure 1**).

**Figure 1.** Building of the HiLASE R&D Centre in Dolní Břežany, Czech Republic.

## 2. High repetition rate picosecond Yb:YAG thin disc-laser in LPP EUV source

Continuous shrinking of the microcircuit is the natural law for lower cost, higher yield, short time to the market in the semiconductor industry. The microlithography has been the central manufacturing technology, and the continuous shrinking of the wavelength is the principal architecture. The proposal of the application of EUV wavelength appeared long before the perspective of the light source itself. The shift of source technology to the ArF excimer is followed by immersion technology and the ArF laser is the long-life light source technology. The EUV lithography is now entering into the mass production phase in the 22 nm node, and the wavelength is 13.5 nm (92.5 eV) supported with Mo/Si high reflectivity mirrors. 13.5 nm wavelength is the first generation of ionizing radiation in the mass production of semiconductor industries. The laser-produced plasma (LPP) EUV source has been established as the basic architecture of the EUV source technology, after one decade of focused research and engineering. The present concern is the stability and cleanness of the source itself and further engineering is continued [22]. The EUV light source is essentially incoherent spherical emission from highly ionized Tin plasma. The source is composed of three parts, namely driving laser, plasma generation/exhaust, and EUV light collector. A large Mo/Si collector mirror has peak reflectivity at 13.5 nm with 2% bandwidth. It is located close to the high-power plasma source and the extension of the lifetime is the most critical engineering concern. It is reported in a recent conference that the power available at the intermediate focus (IF) in the field is 125 W, and a test source is operated in a company laboratory aiming at 250 W [23]. A typical configuration of the LPP EUV source for high volume manufacturing (HVM) is shown in **Figure 2**, where a train of 100 kHz Sn droplet is injected and irradiated by a solid-state laser prepulse

http://dx.doi.org/10.5772/64147

(purple), dispersed into a mist bunch, and irradiated by a $CO_2$ laser main pulse (red). A discharge pumped EUV source is now employed for metrology purpose in less than 100 W level. The typical configuration is shown to the right of the LPP system. A small laser pulse initiates Sn vapor for main discharge from a rotating disc immersed in Sn liquid [24]. It is called as laser-assisted discharge plasma (LDP).

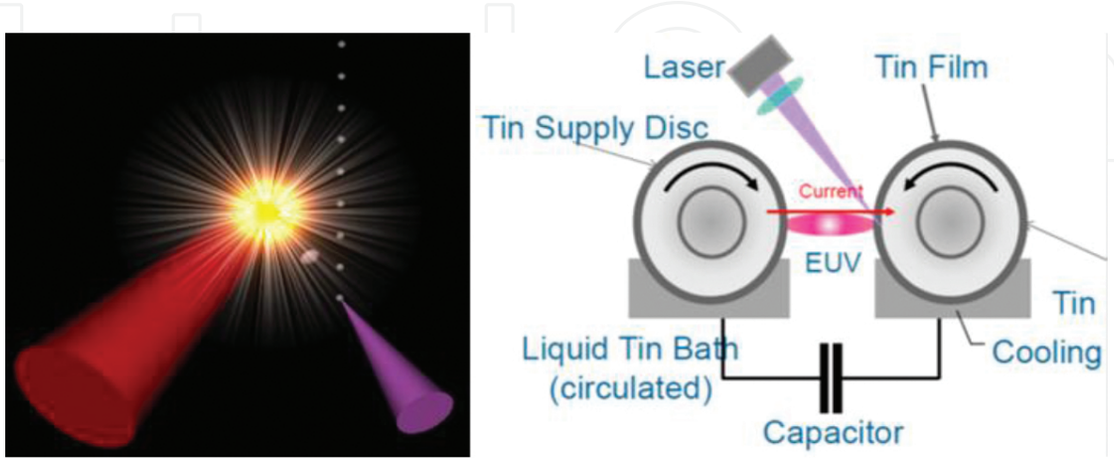


**Figure 2.** Configuration of double pulse method in LPP (left) and LDP (right) EUV sources.

The initial state of the injected Sn droplet is liquid phase of 10–20 μm diameter in the LPP system, and the direct laser irradiation results in a lower conversion efficiency (CE) and messy split of liquid Sn inside the chamber. The solution is the double-pulse method, as the initial pulse converts the liquid Sn droplet into nanocluster bunch (mist) for better laser absorption and ionization. An experiment demonstrated that the prepulse is much efficient in the case of picosecond pulse length compared to the nanosecond one. **Figure 3** shows the experimental results reported in a conference [25].

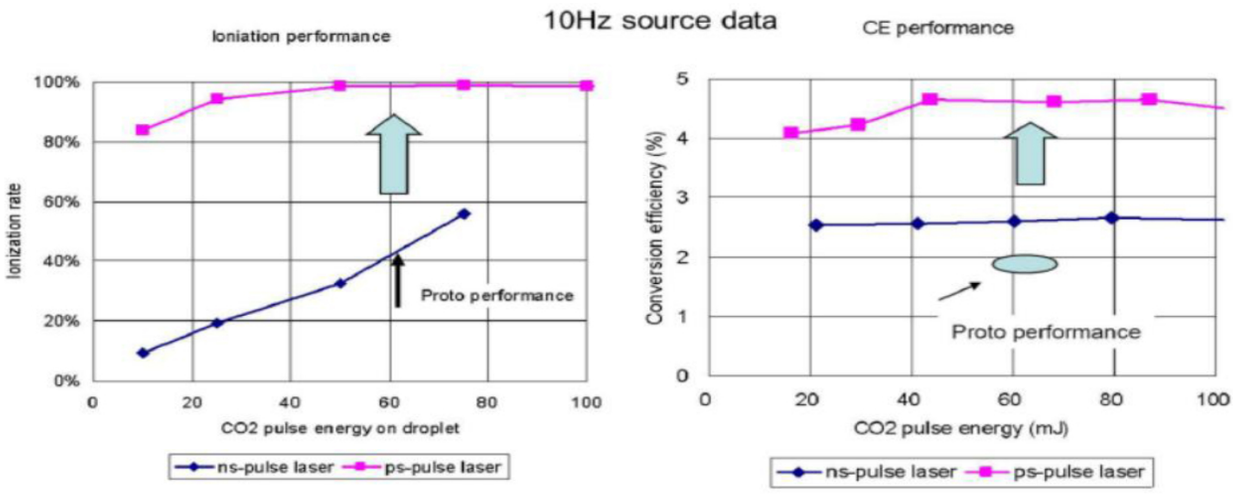


**Figure 3.** Ionization rate of Sn and CE depending on the pulse length of pre-pulse. Left: Ionization rate. Right: Conversion efficiency (CE).

The picosecond laser has typical parameters as pulse energy more than mJ, pulse length is 10 ps or less, and focusing diameter is a few times larger than the droplet diameter of 10–20 μm. The average power is more than 100 W at the repetition rate of 100 kHz. The laser specification is not easily covered by any commercial products and must be specifically developed. Thin-disc laser is suitable for the required specification among other types of advanced lasers such as fiber or thin slab with its larger beam diameter. HiLASE project was dedicated in a research and development of kW class picosecond thin-disc lasers in the period of 2012–2015. One of the laser beamlines is PERLA (Pearl) C, which is aimed to realize a compact, stable 500 W picosecond thin-disc laser with 100 kHz repetition rate [26]. The research and development of the laser system is briefly described in the following.

Design of the laser comes from the thin-disk laser concept. **Figure 4** shows the configuration of the thin-disc laser module with a parabolic mirror that collimates and images the pump radiation from laser diodes. The parabolic mirror images several times the unabsorbed pumping radiation with a set of roof mirrors. The thermal lensing is limited minimum due to the axial thermal flow from the gain medium to the water cooled heat sink. The nonlinear effects in the solid-state medium (self-phase modulation, B-integral) are controlled at low level in the multiple optical passes in the thin disc. The cooling is efficient due to the small thickness of the disc. The typical discs are characterized by the gain thickness as 100–300 μm and the disc diameter as 8–30 mm. Special optical design is required to compensate the low single-pass amplification gain together with pump absorption. Regenerative amplifier is selected for medium-power amplifier, and multipass amplifier is designed for higher average power or higher pulse energy amplifier. Regenerative amplifiers allow very compact and robust laser systems. High-power regenerative amplifier concept is based on a ring cavity, which is in fact a new approach. High average power and high repetition rate regenerative amplifiers usually suffer from Pockels cell issues. A new kind of large aperture BBO Pockels cell was developed to overcome this obstacle (**Figure 4**). A kW-class regenerative amplifier with a ring cavity is a novel approach in the field of picosecond thin disk lasers.

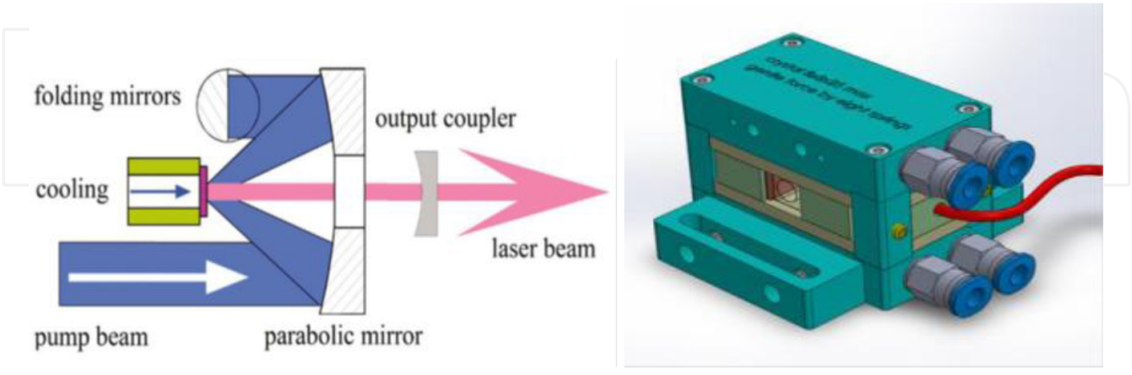


**Figure 4.** Left: Concept of efficient pumping (blue beam) of thin-disk lasers. Right: in-house developed large-aperture and water-cooled BBO Pockels cell.

Various solid-state materials are applied in thin disc modules, and the Yb:YAG is the most favored one due to high quality in fabrication and picosecond pulse generation. Yb:YAG is

http://dx.doi.org/10.5772/64147

studied for more than two decades in its growing, cutting, and polishing, and its thermomechanical characteristic is well fitted for picosecond and subpicosecond pulse generation. One of the disadvantages of the thin-disc laser is the bonding technology of large diameter thin Yb:YAG disc to the heatsink basement to be robust in high-temperature and high optical fluence environment. Several bonding methods are available to 10 mm diameter and further new techniques are still tested for higher reliability. In the present stage, HiLASE Centre uses two types of bonding methods, namely soldering to a copper-tungsten heatsinks and bonding to a diamond substrate. The diamond substrate is advantageous for its higher thermal conductivity for lower disc temperature under high pumping fluence. Popular pumping source is a laser diode with 940 nm center wavelength where the absorption has a broader bandwidth. Yb:YAG has a narrower but high-peak absorption wavelength at 968.8 nm, which is called as zero-phonon line, and a specific laser diode at this wavelength is used for efficient pumping. The quantum defect decreases from 8.7% with 940 nm pumping to 5.9 % with zero-phonon line pumping. Zero-phonon line pumping is also better in its suppression of nonlinear phonon relaxation in the Yb:YAG medium. The resulting steady-state disc temperature is kept lower compared to 940 nm pumping, and better stability of the amplification and higher output pulse energy is the positive result [27]. Pump diodes should have bandwidth <1 nm. Since the absorption line near 968.8 nm is very narrow, the diodes are stabilized by volume Bragg gratings (**Figure 5**).

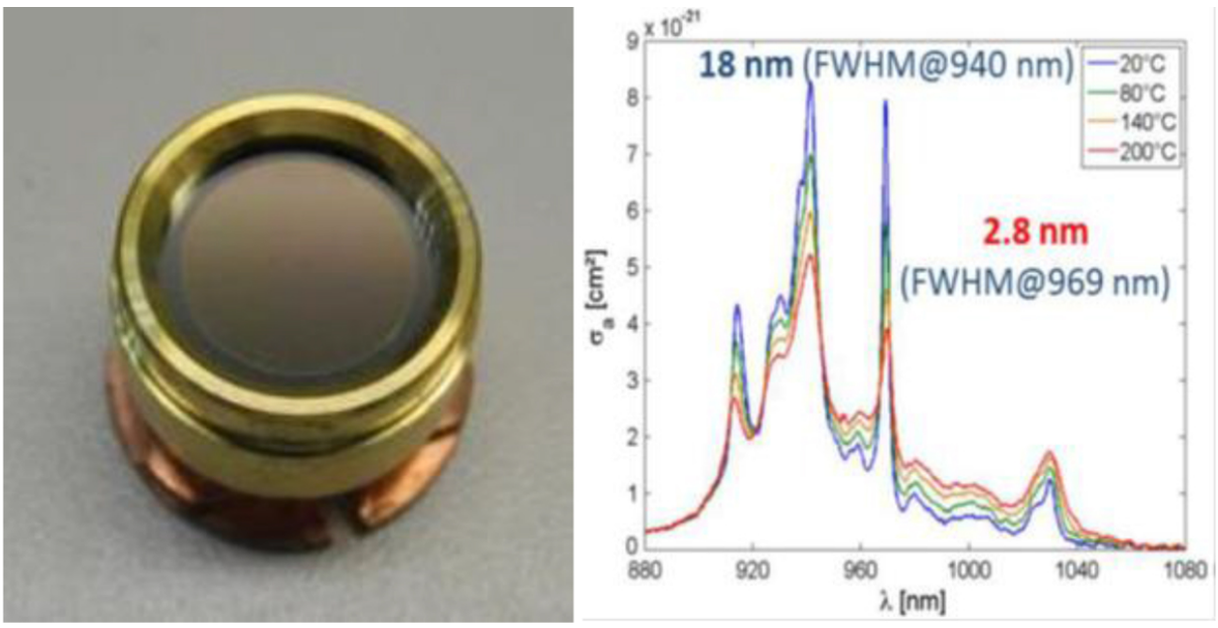


**Figure 5.** Left: Diamond-heat spreader-bonded thin disc. Right: Absorption cross section of Yb:YAG.

The high repetition rate beamline PERLA C operates at 100 kHz and provides picosecond pulses from 1 to >4 mJ in a compressed pulse. The seeder of the laser system is a commercially available Yb-doped fiber laser from Fianium. The pulse length is 12 ps at 50 MHz repetition rate, and the pulse energy is 6 nJ with 20 nm broad bandwidth. The pulses are stretched to 0.5 ns pulse length by a small Bragg grating. The pulse bandwidth is filtered to 2.2 nm by the

bandwidth of the grating, and the bandwidth limited pulse length is less than 2 ps. The seeder pulses are amplified by a semiconductor optical amplifier (SOA) and a single-mode fiber amplifier before injection into a regenerative amplifier. The advantage of the SOA is its electric controllability of the gain time window and used as a pulse picker to reduce the repetition rate from 50 to 1 MHz. The average power is 300 mW before the regenerative amplifier.

The regenerative amplifier is composed of a single Yb:YAG module with a standing wave cavity for 100 W operation (**Figure 6**). The total footprint is compact as 900 × 1200 mm including a pulse compressor. The pump spot size of the thin disc is 2.7 mm in diameter with cavity length of 2 m. A double Pockels Cell system optically switches the input and output pulses. The size of the BBO crystal is 8 × 8 $mm^2$. The crystal holder is engineered to avoid damages to the BBO by piezo ringing in high repetition rate switching. The maximum available BBO aperture is 12 × 12 $mm^2$, and the repetition rate is 1 MHz and the voltage is 10 kV. As described earlier, the pumping is by zero-phonon line continuous fiber-coupled laser diodes. The maximum amplified pulses are 1.2 mJ of energy at 100 kHz repetition rate with M2 = 1.3 beam quality

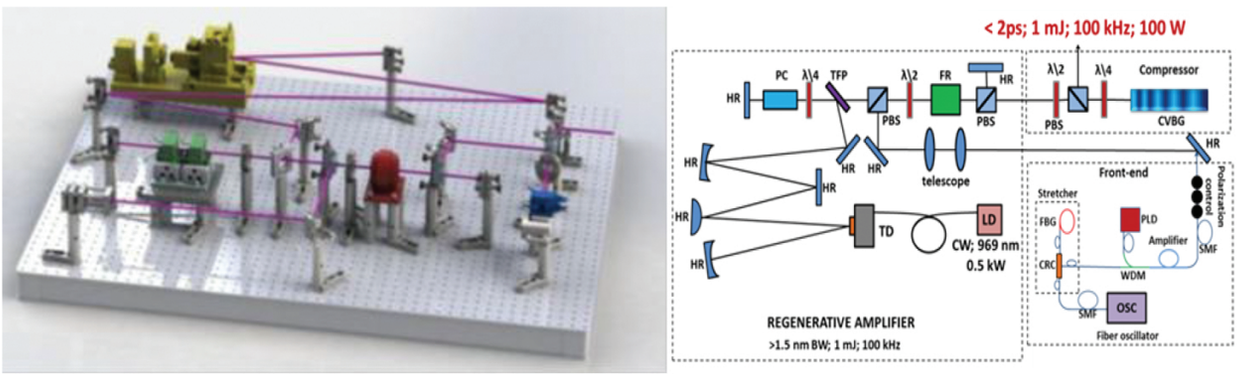


**Figure 6.** Left: 100 W regenerative amplifier. Right: Optical scheme including a CVBG pulse compressor (HR, highly reflective mirror; TD, thin disk; LD, pump laser diodes; PC, Pockels cell; TFP, thin-film polarizer; FR, Faraday rotator; PBS, polarizing beam splitter; CVBG, chirped volume Bragg grating; $\lambda/2$ and $\lambda/4$, half- and quarter-wave plates; SMF, single-mode fiber; PLD, pump laser diode; WDM, multiplexer; CRC, circulator; FBG, fiber Bragg grating; OSC, oscillator).

This is critically important for precise irradiation like prepulse in an LPP EUV source. Pulses are compressed by a chirped volume Bragg grating (CVBG) compressor, which is a very robust, compact, and easy to align bulk compressor with 8 × $8^2$ mm aperture. The CVBG compressor was tested for long time operation and demonstrated a reliable pulse compression of high average power pulse train with >85 % diffraction efficiency under optimized cooling condition. Compressed pulses measured by intensity autocorrelation (**Figure 7**, right) have temporal width 1.6 ps ($sech^2$). The pulse-to-pulse energy stability measured over 4 million pulses was better than 1.7%, and the long-term average power stability measured over 1 h was <1.5 % (RMS value). Better housing and active stabilization can even improve the stability.

http://dx.doi.org/10.5772/64147

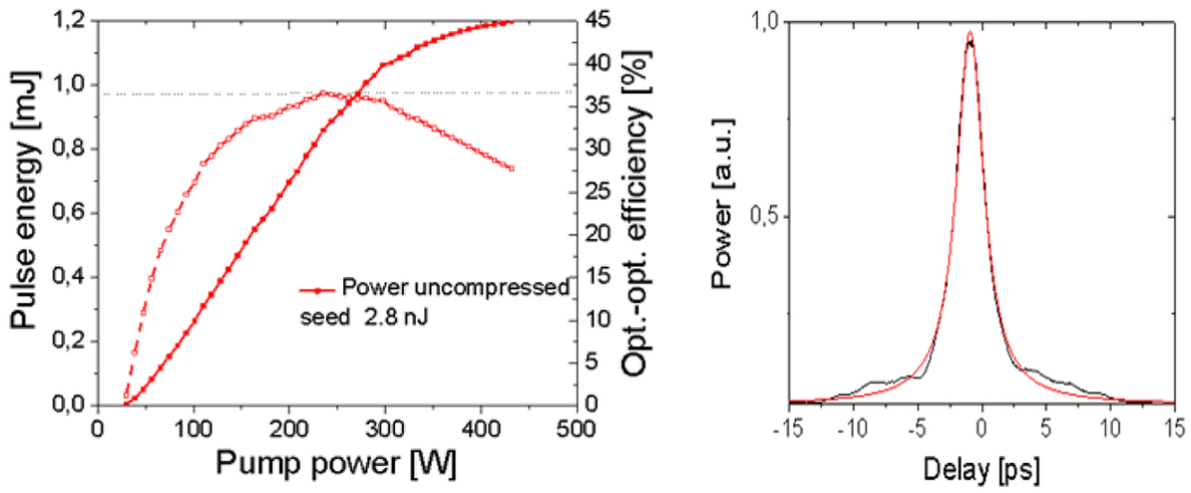


**Figure 7.** Left: 1.2 mJ of the output pulse energy at 100 kHz repetition before compression has been achieved from the 100 W PERLA C in a nearly diffraction-limited beam. Right: the pulses were compressed to 1.6 ps (FWHM) by a CVBG as shown by the intensity autocorrelation trace.

A higher average power regenerative amplifier was developed with a ring cavity (**Figure 8**). The amplifier is switched by a reliable Pockels cell, which is in-house design for 10 × 10 mm$^2$ aperture with effective cooling. The fundamental spatial mode operating cavity is designed for a 5.2 mm pump spot and the cavity contains a single diamond-bonded Yb:YAG thin disc. The disc is zero-phonon line-pumped by VBG-stabilized fiber-coupled diodes. Laser cavity was tested in the CW regime to evaluate the thermal distortion. 550 W output was observed with almost 50% optical-optical efficiency and >4 mJ was achieved in a 100 kHz pulse train with a nearly diffraction-limited output beam (**Figure 8**).

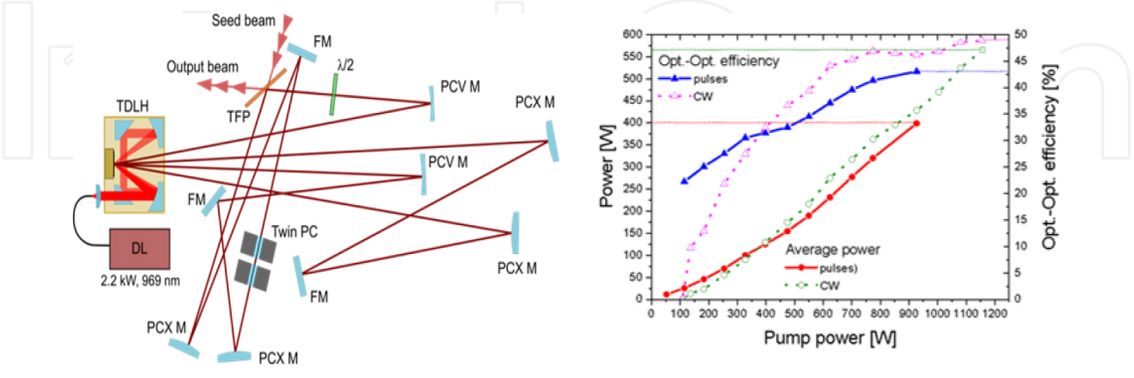


**Figure 8.** Left: ring cavity of the 500 W PERLA C laser system. FM, folding mirror; PCX M, planoconvex mirror; PCV M, planoconcave mirror; TFP, thin-film polarizer; PC, Pockels cell; TDLH, thin-disc laser head; DL, pump diodes; λ/2, half-waveplate. Right: performance of the 500 W ring cavity in CW and pulse mode (PERLA C).

## 3. High average power wavelength conversion of picosecond solid-state lasers

The extreme ultraviolet lithography is now in an introductory phase in semiconductor industry. The EUVL has been developed in the field of various component technologies such as Mo/Si high reflectivity mirror at 13.5 nm wavelength, new types of resist of higher sensitivity at this wavelength, and plasma-based 100 W class stable EUV sources. Further increase in average power is expected for large-scale manufacturing to kW level and shorter wavelength to 6.7 nm where a higher reflectivity mirror seems available. The present source architecture is the laser-produced plasma (LPP) and is recently considered in its practical scaling limitation in average power in the range of kW. Free electron laser has been emerging as the new short-wavelength source in the EUV to X-ray region in the past decade. The present generation is based on lower repetition rate operation for scientific applications, but the next generation is aiming at high repetition rate for high average power. Several research papers are discussing on the possibility of high repetition rate FEL by superconducting RF cavity technology for the generation of more than kW average power at 13.5 nm wavelength [28, 29]. The present FEL is operated in the SASE mode, in which the pulses are generated in undulator and composed of many short-pulse length spikes. The typical pulse parameters are 0.1 mJ pulse energy, 100 fs pulse length, and the beam diameter is 1 mm. The beam fluence is higher than the ablation threshold of a resist [30], and the high spatial coherence results in much higher localized peak fluence on the resist. The interaction mechanism is now in a basic study to overcome these effects compared to the present LPP-generated 100 kHz, mJ EUV pulses with no coherence and longer pulse length as 10 ns.

The scaling of the FEL technology to kW average power level requires the photocathode operation in higher repetition rate in industrial environment together with optical technology to optimize the FEL beam for lithography application and scaling to the 6.7 nm wavelength region.

The first consideration is the industrial operation of photocathode at >MHz repetition rate. The bunch charge is typically 1 nC. Metal photocathode is robust, but the quantum efficiency (QE) is lower for higher charge generation. Several semiconductor cathodes were studied for higher efficiency to reduce the requirement for the driver laser average power in the repetition rate mode. The Advanced Photo-Injector (APEX) experiment in Lawrence Berkley National Laboratory is working to realize a high repetition rate at MHz, high-brightness photocathode. The photocathode is a normal conducting, 187 MHz RF cavity in the CW mode, and designed for short bunches as 1–10 ps of 750 keV energy up to 1 nC charges. Several semiconductor cathode materials are tested for better beam emittance for various operational conditions. $CsK_2Sb$ is irradiated by SHG of Yb fiber pulses, and $Cs_2Te$ is irradiated by 4HG. Both semiconductor cathodes have nearly 1% quantum efficiency. The laser pulse energy is 0.5 μJ with the MHz repetition rate, and the average power is 0.5 W [31]. Cu and Mg photocathodes were studied for use in an RF photocathode. The gun was manufactured by a technique of hot isostatic pressing with diamond polishing and tested under a peak electric field of 57 MV/m. The quantum efficiency of the Cu cathode was $10^{-4}$, while Mg cathode achieved a high QE of

http://dx.doi.org/10.5772/64147

up to $10^{-3}$ under 262 nm laser-light illumination. The QE of the Mg cathode under 349 nm laser-light illumination was measured to be $2.2 \times 10^{-5}$. The experimental setup and the results of the photocathode QE measurement are shown in **Figure 9** [32].

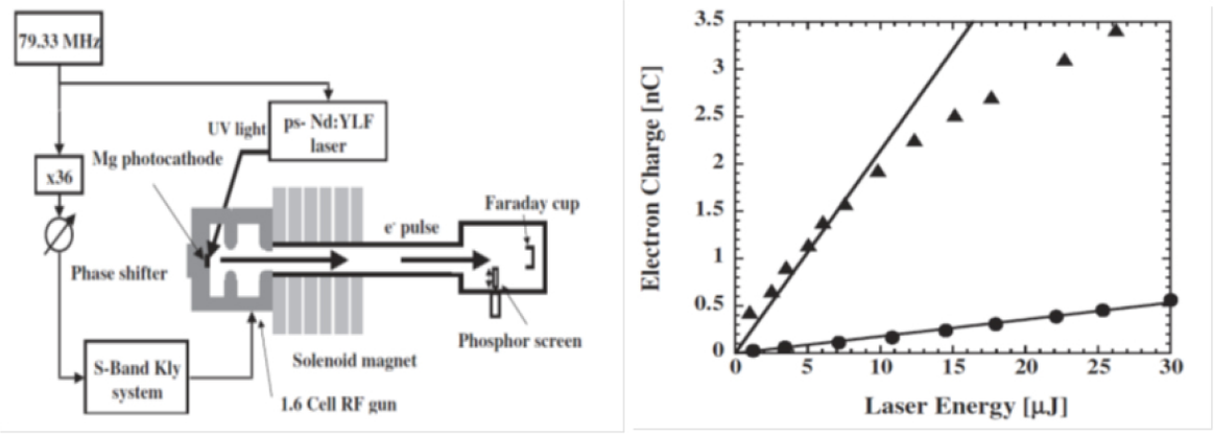


**Figure 9.** Left: Experimental setup of photocathode QE measurement. Right: Electron charge vs. input laser energy (266 nm) from Mg photocathode, • is for before laser cleaning.

It is concluded that 5 μJ, 266 nm, picosecond pulse is enough for Mg photocathode operation and the required average power at the MHz repetition rate is 5 W. Cu photocathode is proven to be robust material and usable by a 50 W 4HG picosecond laser. The progress of the laser technology is now making the metal photocathode again usable for the emerging requirement for long-life industrial application.

The other consideration is the reduction of the temporal microspikes in the SASE FEL pulses. Coherence is characterized in a report on the FLASH operation at 8.0 nm wavelength [33]. The single FEL femtosecond beam is passed through double pinholes for diffraction pattern, and the measured transverse coherence length is 6.2 ± 0.9 μm in the horizontal and 8.7 ± 1.0 μm in the vertical directions. The mutual coherence function K is given as 0.42, and a measurement of K by a laser plasma source is $3.2 \times 10^{-9}$. It is concluded from these measurements that a beam spatial homogenization is required at EUV wavelength by using total reflection. Temporal coherence was also reported by using a split and delay unit. The coherence time of the pulses produced in the same operation conditions of FLASH was measured to be 1.75 fs. The measured coherence time has a value, which corresponds to about 65.5 ± 0.5 wave cycles ($c\tau/\lambda$). It is well known that the SASE FEL pulses are composed of many small spikes and random spectrum due to SASE process. It is reported that the averaged spectrum has a 1.4% bandwidth typically, which is favorable for the Mo/Si EUV multilayer mirror at 13.5 nm (bandwidth 2%). It is necessary to smooth the temporal spikes to avoid random EUV flux change in the resist absorption process. The requirement is similar to most FEL applications, and we must consider efficient seed technology for MHz repetition rate operation.

It is desirable to increase the brightness and pointing/energy stability compared to SASE mode. An efficient seeding method was established by using a UV wavelength laser, in which the seed laser modulates the electron beam into coherent bunching at the harmonics of the seed

laser wavelength. The bunching is intensified in another undulator for coherent FEL action, and the method is called as high-gain higher harmonic generation (HGHG). FERMI is the leading institute in this specific technology, and it is reported on the double-stage-seeded FEL with the fresh bunch injection technique [13]. The main limitation for the direct extension of the HGHG to shorter wavelength is the required small electron beam energy spread and higher average power seed laser source. The fresh bunch scheme is the solution for this problem, in which the FEL radiation is initially produced in an earlier stage undulator and used as the seeder for shorter wavelength generation (**Table 1**).

| | **Fermi FEL-2** | **EUV FEL** |
|---|---|---|
| Seed wavelength (nm) | 260 | 324 |
| 1nd FEL (nm) | 32 | 40.5 |
| 2nd FEL (nm) | 10.8 | 13.5 |

**Table 1.** Comparison of wavelengths for HGHG operation in FERMI FEL-2 and EUV FEL.

The external seed laser was the third harmonic of a Ti:Sapphire laser with a duration of ~180 fs (FWHM) and up to 20 μJ energy per pulse. Its transverse size in the modulator was made larger than the electron beam size to ensure as uniform as possible electron beam energy modulation. Once the same laser energy is required for MHz EUV FEL, 20 W average power is required for 324 nm with 180 fs at MHz repetition rate. There are two approaches to generate such laser pulses, the first is based on the MHz repetition rate Ti:Sapphire laser with 100 μJ level pulses, and the second one is based on OPCPA.

The short-pulse, short-wavelength laser technology is now advancing to realize the specification described here in a compact box, due to the new suitable laser configuration as thin-disc laser and an efficient wavelength conversion method.

An ultrafast thin-disc multipass laser amplifier demonstrated the advantage recently by delivering 1.4 kW of average output power with 4.7 mJ pulse energy and duration of 8 ps at a repetition rate of 300 kHz [18]. The beam quality factor was better than M2 = 1.4. The experiments show that the thin-disc multipass amplifier can scale pulse energy and average output power independently for the investigated repetition rates between 300 and 800 kHz. Frequency doubling by means of an LBO crystal generated 820 W SHG average power at the wavelength of 515 nm with 1170 W of incident IR power, which corresponds to a conversion efficiency of 70% and an SHG pulse energy of 2.7 mJ. By sum-frequency generation between the beams at 1030 and 515 nm in a second LBO crystal, an average UV power of 234 W (780 μJ of pulse energy) was generated at the wavelength of 343 nm THG with a conversion efficiency of 32%.

A wavelength conversion experiment was performed in the HiLASE project to evaluate the high average power generation of picosecond harmonics, namely, SHG (515 nm) and FHG (257.5 nm), in LBO and BBO/CLBO crystals, respectively [34]. The pumping of the crystals was performed by the PERLA C Yb:YAG thin-disc laser operating at 100 kHz and 60 W average power with 4 ps pulse duration. The average output power of 6 W DUV was achieved in CLBO

http://dx.doi.org/10.5772/64147

at a spectral bandwidth of 0.2 nm and the FHG/fundamental conversion efficiency was 10%. The basic optical configuration is shown in **Figure 10** together with a photo. The input beam (upper left) is reflected by two motorized mirrors controlled by a beam stabilizer ensuring pointing stability better than 20 μrad (RMS). The following half-wave plate and polarizer is used for energy tuning. The beam is frequency doubled in an LBO at 50°C and 10 mm long, cut for the critically phase-matched generation at $\theta = 90°$ and $\phi = 12.8°$, and antireflection coated for 1030 and 515 nm. The second harmonic beam passes two dichroic mirrors and is injected into an argon-filled box with a BBO or CLBO crystal. To ensure a stable long-term functioning of the crystals the temperature was kept at 150°C. The experimental results are shown in **Figure 11**. It is visible that the 4HG/SHG conversion in the CLBO crystal has 30% higher efficiency than in the BBO crystal. The next step of the experiment is to increase the pumping power to 500 W to confirm the linearity of the conversion efficiency for 50 W FHG output power.

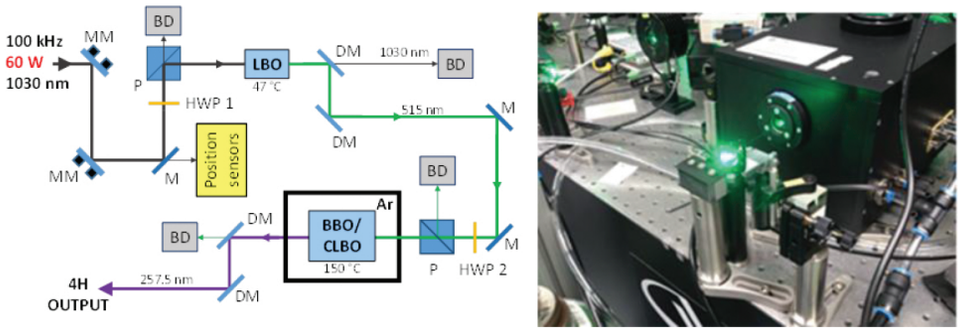


**Figure 10.** Optical configuration of the SHG and FHG, and SHG light is introduced into a box filled with argon.

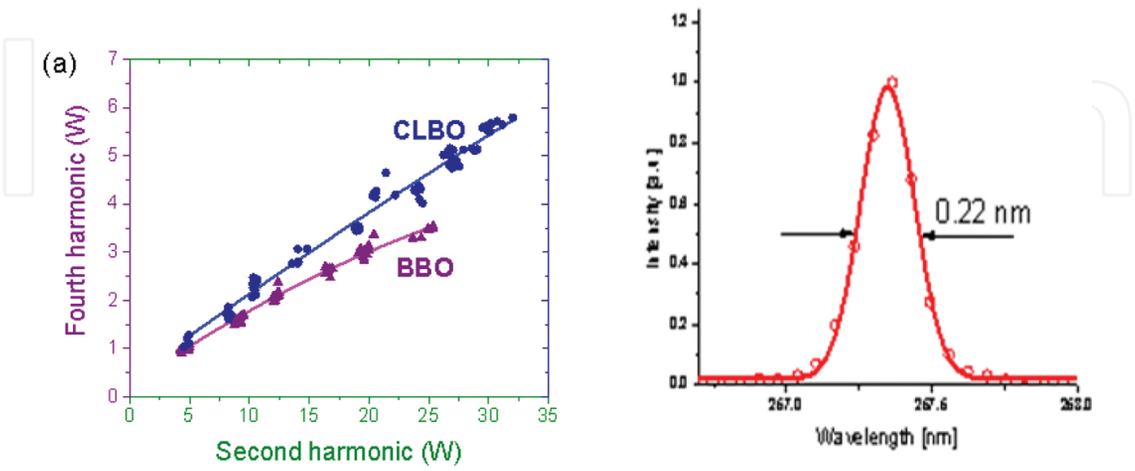


**Figure 11.** Left: Fourth harmonic output power dependence on the second harmonic in BBO (AR coated) and CLBO (uncoated) crystals. Right: Relevant FHG spectra from CLBO.

A small part of the beam is absorbed in the crystal and converted into heat that leads to temperature gradients in the crystal in the high average power wavelength conversion. This causes partial phase mismatch and reduces the conversion efficiency. It is estimated that the fundamental power absorption at the 60 W input is <20 mW in the 10 mm long LBO crystal. The total absorbed power may be higher due to the fact that a green laser beam has higher absorption than the fundamental beam [35]. The absorption in the antireflective coating increases the temperature, which causes the mismatch more than the bulk absorption [36].

A tunable, 112 W optical parametric chirped-pulse amplifier (OPCPA) was demonstrated for FEL seeding in a burst mode with center frequencies ranging from 720 to 900 nm, pulse energies up to 1.12 mJ, and a pulse duration of 30 fs at a repetition rate of 100 kHz [14]. The results demonstrated the feasibility of 112 W femtosecond OPCPA in a burst mode with a duty cycle of $8 \times 10^{-3}$, where no heating effects were observed. It was indicated from the measurements of absorption coefficients of BBO and LBO and calculations, the feasibility of much higher powers up to 1 kW in continuous mode was expected. Absorption causes a spatially and temporally varying temperature distribution in the sample. This leads to local changes of the refractive index and results in the development of a thermal lens. Especially in anisotropic crystals, this has consequences on increased phase mismatch in optical parametric processes with a conversion efficiency decrease. In the case of anisotropic crystal in electro-optical devices such as Pockels cells, the thermally induced depolarization reduces the contrast ratio. Though the absorption of the anisotropic crystal in these applications is usually very low, the related effects can be significant with input powers at the kilowatt level. In order to estimate the influence of thermal effects and taking it into account in the optical system design, the comprehensive knowledge of material absorption at the operation wavelength is unavoidable. An extended photothermal method was demonstrated for the quantitative determination of laser-induced wavefront deformations, which enables the separation of bulk and surface contributions to absorption in the more complex case of optically anisotropic crystalline media [36]. Experimental setup is shown in **Figure 12**. The wavefront deformations of the test beam (light source) are measured and used for absorption evaluations. The results show that the absorption is highest at the AR-coated KTP surface of input side (**Figure 13**, left), while it is higher at the surface of the output side of noncoated KTP (**Figure 13**, right). This photothermal method is usable in the real OPCPA for a better cooling system installation.

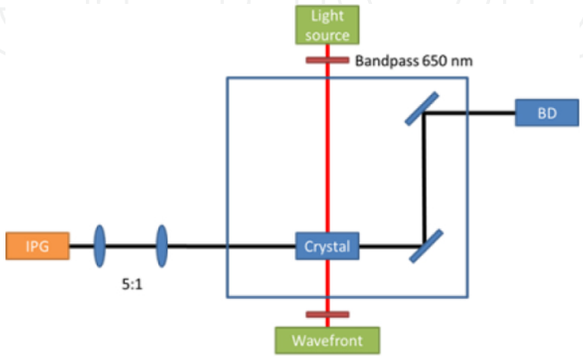


**Figure 12.** Setup of the photothermal method by crossed beam measurement. Wavefront measurement is performed by a Hartmann-Shack sensor.

http://dx.doi.org/10.5772/64147

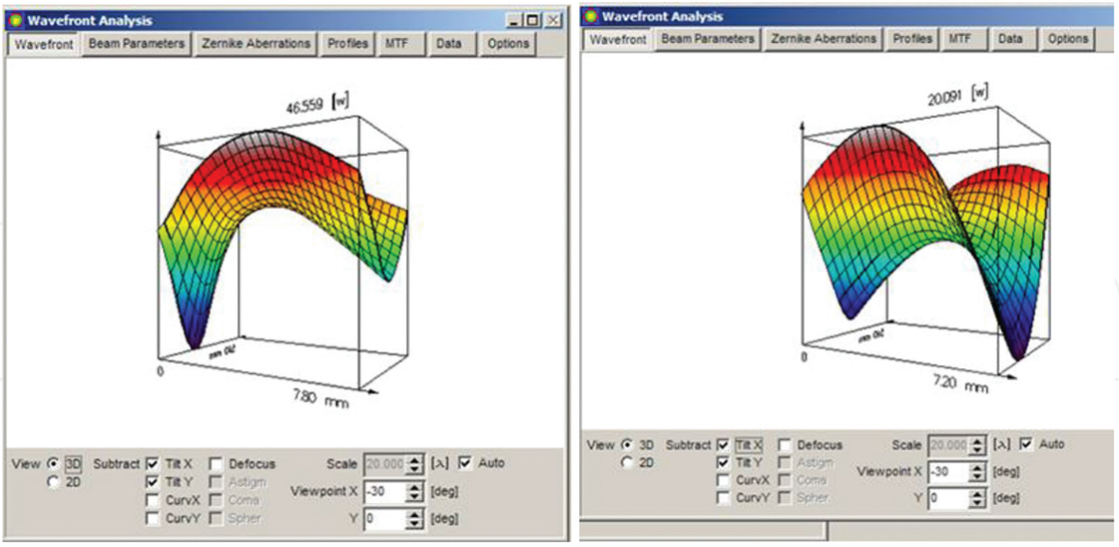


**Figure 13.** Wavefront deformation measurement results for AR-coated (left) and noncoated KTP samples. Blue indicates the largest wavefront deformation. The heating laser beam comes into the crystal horizontally from the left, while the probe beam passes vertically to the readers.

## 4. Cryogenic laser technology for high pulse energy picosecond amplifier

The basic principle of the laser Compton short-wavelength source is similar to an undulator emission, and high-intensity laser field is used as the modulating electromagnetic field. Basic principle of the laser Compton X-ray source is well studied, and a single-shot imaging is critical for many practical applications. The required specification is explained as the laser pulse must exceed some threshold parameters. It is known that the highest peak brightness is obtained in the case of counterpropagating laser pulse and electron beam bunch, in the minimum focusing area before nonlinear threshold. **Figure 14** describes the schematic of the laser Compton interaction between the electron beam and the laser.

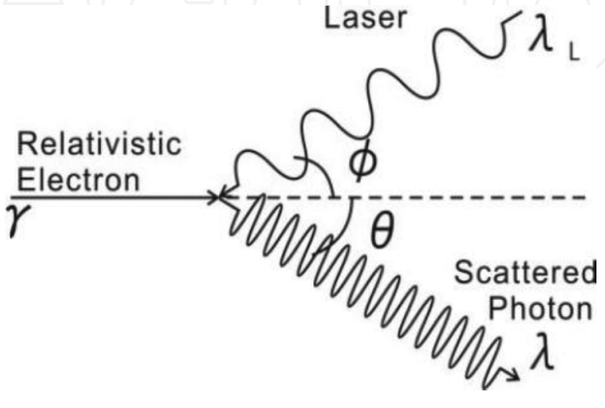


**Figure 14.** Schematic of the laser Compton scattering process.

The general formula of obtainable X-ray photon flux $N_0$ is calculated in the counter collision by the following expression:

$$N_0 \infty (\sigma_c \, Ne \, Np) / (4\pi r^2)$$

where $\sigma_c$ is the Compton cross section ($6.7 \times 10^{-25}$ cm$^2$), Ne is the total electron number, Np is the total laser photon number, and $r$ is the interaction area radius. It is predicted that an increase in Ne and Np, and the reduction in $r$ results in the increase in the photon flux $N_0$. The practical limitation of these operations are the instrumental condition of electron beam emittance in higher charge, M2 of laser beam at higher pulse energy, and optimization for reduced focusing diameter $r$. It is possible to assume these parameters as 1 nC charge with 3 ps pulse duration to be focused down to 10 μm at 38 MeV voltage. Another limitation is the maximum of single-pulse laser intensity to reach the nonlinear threshold of the higher harmonics generation in the X ray region. The nonlinear Compton threshold is characterized by the laser field strength

$$a0 = eE/m\omega LC$$

where parameters $E$, $\omega$L, and $C$ correspond to the amplitude of the laser electric field, laser frequency, and the speed of light, respectively. The laser field strength is a function of the laser wavelength. The nonlinear threshold $a_0$ is given around 0.6 which corresponds to 1 J pulse energy in 1 ps pulse duration at 10 μm focusing intensity in the solid-state laser wavelength. The threshold laser energy for a single-shot imaging is similar to this critical laser pulse energy in the expected tight focus condition. The laser technology was not matured to realize such parameters simultaneously in the past, and usual approach was to increase the repetition rate of the event to increase the effective obtainable X-ray photon average flux in the affordable imaging time period such as <millisecond for bioimaging. The first approach is the pulsed laser storage in an optical enhancement cavity for laser Compton X-ray sources [37]. It is described in the experimental report that "the enhancement factor $P$ inside the optical cavity was 600 (circulating laser power was 42 kW), in which the Finess was more than 2000, and the laser beam waist of 30 μm (2σ) was stably achieved using a 1 μm wavelength Nd:Vanadium mode-locked laser with repetition rate 357 MHz, pulse width 7 ps, and average power 7 W." The second approach is the multipass optical cavity, in which the laser Compton generation focus exists inside the multipass cavity. The minimum focusing diameter is limited due to the requirement of the cavity design. SHG picosecond pulse of 0.2 J pulse energy is circulated 32 times to collide electron bunches [38].

An approach is undertaken by the thin-disc laser technology to generate 1 J, picosecond high beam quality pulses at 100 Hz repetition rate in the Max Born Institute, Berlin, Germany. The development is based on a ring cavity concept combined with chirped pulse amplification (CPA) [39]. The regenerative amplifier produced more than 300 mJ energy when pumped with the maximum available pump power of 1.7 kW. The regenerative amplifier is followed by a large aperture ring amplifier that increases the pulse energy further to 600 mJ. This ring

http://dx.doi.org/10.5772/64147

amplifier consists of a Pockels cell and a set of polarizers for the in- and out-coupling, two amplifier heads and a spatial filter in between. The amplifier heads are equipped with 750 μm thick Yb:YAG (7%) discs of 25 mm diameter. Each disc is pumped by 1 ms long pulses of 4 × 1.5 kW. Booster amplifier for 1 J pulse is based on the large aperture ring amplifier design without internal Pockels cell. The amplifier discs were pumped by diode modules that deliver 6 kW peak power out of a 2 mm fiber. Each amplifier is equipped with two of these pump modules, which together provide about twice the pump power compared to the large aperture ring amplifier. The booster amplifier is changed from former multipass configuration to a large aperture ring amplifier. The result is a multiple amplifier stage configuration with many thin-disc laser modules.

Cryogenic laser technology is suitable for the generation of large-pulse energy in a laser configuration of lower stages. A cryogenic thick-disc Yb:YAG laser was reported as 1 J was generated at 100 Hz repetition rate [3]. The picosecond CPA laser was developed for driving high average power soft X-ray lasers. This is one of the greatest breakthroughs in the history of high-energy solid-state laser, and it is described in the report on the configuration and operation as "Seed pulses of 100 mJ energy were produced by the laser frontend and amplified to 1.5 Joules pulse energy by the five-pass power amplifier which consists of two Yb:YAG disks mounted in vacuum on a single cryo-cooling head. The Yb:YAG disks are bonded on all lateral sides with a Cr:YAG cladding to eliminate feedback of spontaneous emission into the active region to prevent amplified spontaneous emission (ASE) losses and transverse parasitic lasing. Cryogenic cooling of Yb:YAG to liquid nitrogen temperature increases the heat conductivity and reduces the saturation fluence, allowing for efficient high energy pulse generation at high repetition rates. High capacity cooling was accomplished by flowing cryogenic liquid coolant through the laser head. Each disk was pumped with 1.5 ms duration, 4 kW pulses from a $\lambda$ = 940 nm laser diode array. At the maximum pump power, 1.5 J laser pulses were obtained. These pulses were compressed by a dielectric grating pair producing 1 J, 5 ps FWHM duration pulses at 100 Hz repetition rate." The repetition rate is recently increased to 500 Hz and the picosecond pulse energy is 1 J, and the resulting average power is 500 W. Temporally pulse-shaped laser pulses were focused into a ~5 mm long, 30 μm FWHM wide line on a solid target using cylindrical optics. The beam quality is indicated by the focusing specification. The resulting plasma was in the Ni-like stage, and strong collisional excitation leads to a large transient population inversion on the $4d1S_0 \rightarrow 4p1P_1$ transition of Ni-like ions at wavelengths ranging from 10.9 to 18.9 nm.

Cryogenic solid-state laser is preferred for power scalability with better beam quality, especially in higher pulse energy mode, and improvement of efficiency at the cost of longer pulse length [40]. Yb:YAG is the most tested material due to its low quantum defect and still broadband absorption in low temperatures. Various thermal optical properties are reported for base materials as YAG (ceramic and single crystal), GGG, GdVO4, and $Y_2O_3$ on the thermal conductivity, thermal expansion, refractive index, absorption cross section, emission cross section, and fluorescence lifetime in the cryogenic condition.

One of the key features of the cryogenic laser is its better beam quality. A quantitative evaluation is important for a practical laser design for dedicated applications and a measure-

ment was performed on the wavefront distortion caused by the thermal origin in a cryogenic Yb:YAG crystal in the temperature range 250–130 K in nonlasing condition [41]. The wavefront aberration was evaluated by a wavefront sensor. The measurement results showed a significant reduction of the wavefront aberration in lower temperature. The thermal defocus was concluded as originated to the thermal lensing effect together with electronically induced change of the refractive index by the excitation of ion activators (electronic lensing). The dominant reason of the aberration was found as the thermal lensing in the experimental condition as 6.3 kW/cm$^2$ pumping intensity and pumping repetition rate of 100 Hz. The Strehl ratio was observed to be improved in the lower temperature even the absorbed energy was increased. The experiment showed the advantage of the cryogenic technology in terms of efficiency and beam quality.

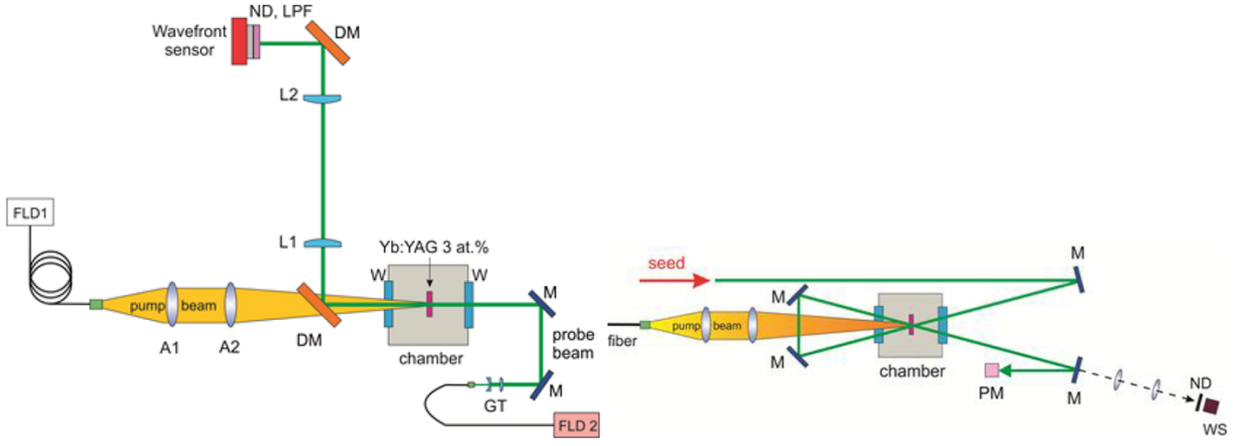


**Figure 15.** LEFT: Experimental configuration of the aberration measurement. FLD1, fiber-coupled pump diode at 936.6 nm; FLD2, fiber-coupled probe beam laser diode at 1065 nm; GT, Galilean telescope; W, windows; M, turning mirrors; DM, dichroic mirrors; A1, 2, achromatic doublets with focal lengths of 100 and 250 mm, respectively, L1, 2, lenses with a focal length of 250 mm; ND, neutral density filters; LPF, longpass filter with cutoff wavelength at 1050 nm. Right: Multipass amplification configuration. WS, wavefront sensor; PM, power meter.

The experimental setup used for the measurement of the wavefront aberrations in a cryogenically cooled Yb:YAG slab is shown in **Figure 15** (left). The right side figure shows the configuration of multipass amplification from the 100 mJ level input. A Yb:YAG crystal is mounted in a copper holder in a closed-loop pulse tube cryostat (Q Drive). The cooling capacity is 12 W at 100 K. The crystal was supplied from Crytur, Czech Republic, and the specification was thickness 2 mm, diameter 10 mm, and doping concentration 3 at%. A fiber-coupled laser diode (DILAS) pumped the crystal from one side. The peak wavelength was 936.9 nm, and the peak intensity was 6.3 kW/cm$^2$. Two achromatic doublet lens of focal length 100 and 250 mm imaged the 1 mm core of the fiber with NA 0.22 to the Yb:YAG surface. The resulting pump spot size was 2.5 mm (1/e2) in super-Gaussian intensity distribution. **Table 2(a)** summarizes the absorbed energy per pump pulse at each temperature. The absorbed energy increases by about 19 % if the temperature decreases by 120 K from initial 250 K. The absorbed power and thus generated heat is higher with decreasing temperature, and the aberrations are lower because of higher thermal conductivity, lower d$n$/d$T$, and lower expansion

http://dx.doi.org/10.5772/64147

coefficient. Theoretical thermal decay time constants were calculated according to the formula $t_T = r_p^2/4\kappa$, where $r_p$ is the radius of the pump, and $\kappa$ is the thermal diffusion coefficient, which is defined as $k/(\rho cp)$ where $k$ is the thermal conductivity, $\rho$ is the mass density, and cp is the specific heat. The estimated values are shown in **Table 2(b)** for the thermal relaxation time constants for different temperature conditions in 3 at% doped Yb:YAG as an estimation from data for 2 and 4 at% doped crystals. The thermal decay time is around 31 ms at 150 K, which is three times longer than the time interval between pumping at 100 Hz. This value is 93 ms at 250 K.

**(a)**

| Temperature (K) | Absorbed energy (mJ) | Absorbed energy (%) |
|---|---|---|
| 250 | 128 | 41.3 |
| 210 | 137 | 44.3 |
| 170 | 145 | 46.8 |
| 130 | 152 | 49.0 |

**(b)**

| Temperature (K) | Thermal decay time for 3 at% Yb:YAG crystal (ms) |
|---|---|
| 250 | 93 |
| 200 | 60 |
| 150 | 31 |

**Table 2.** (a) Absorbed energy per pump pulse by the 2 mm thick, 3 at% doped Yb:YAG slab pumped by energy of 310 mJ at a wavelength of 936.6 nm for different temperatures of the cooling finger. (b) Calculated thermal decay time for 3 at% Yb:YAG crystal.

Cryogenic cooling is usually applied in booster amplifiers with more than one pass of the seed beam through the active medium in order to efficiently extract the stored energy. Therefore, it is assumed to evaluate four beam passes, and the measured wavefront with subtracted tilt and defocus was four times multiplied to calculate the real Strehl ratio in multipass amplification. The calculated Strehl ratio was 0.96 at 130 K and decreased to 0.93 at 250 K as shown in **Figure 16**. The practical Strehl ratio to obtain the same pulse energy decreases at higher temperature to obtain the same pulse energy in lower gain. The measurement indicates the linearity of the Strehl ratio to the temperature decrease, and it is expected further increase in the beam quality is possible in lower temperature of about less than 130 K.

In the last part of this chapter, a large aperture cryogenic laser is evaluated. The performance of a gas-cooled multislab laser is recently reported from the DiPOLE project within the Central Laser Facility (CLF RAL STFC), UK. The development is aiming at an efficient high pulse energy diode-pumped solid-state laser (DPSSL) architecture based on cryogenic gas-

cooled, multislab ceramic Yb:YAG amplifier technology. A prototype amplifier is delivering up to 10.8 J pulse energy at 1030 nm wavelength with 10 Hz repetition rate. The optical-optical conversion efficiency is 22.5% [42]. The long-term energy stability was observed as 0.85% RMS with 7 J pulse energy for 48 h operation (2 million shots). An extension of the cryogenic technology is now under test in the DiPOLE 100 to confirm the cryogenic concept at 100 J, 10 Hz region (kW average power). The present laser system is built for the HiLASE project and will deliver 100 J temporally shaped ns pulses at 10 Hz with a fully integrated control system. A second system is also under development for the high-energy density (HED) beamline of the European XFEL project.

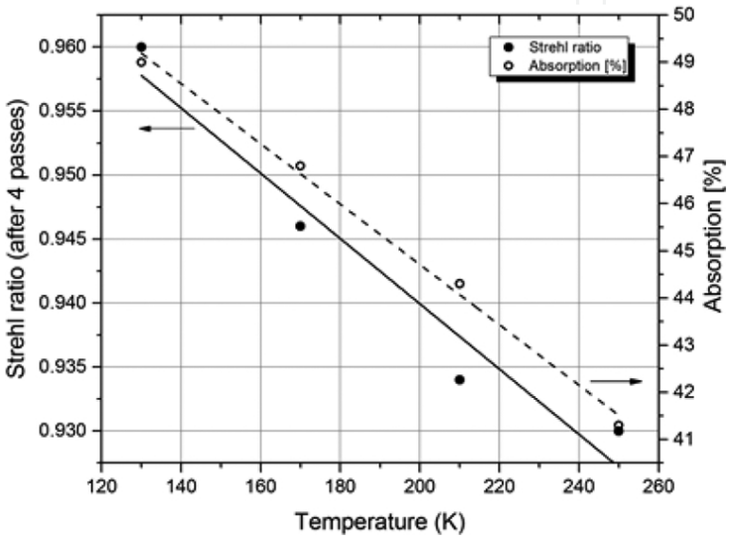


**Figure 16.** Strehl ratio for the four passes of the probe beam through the Yb:YAG slab and absorbed pump power per single pass as a function of temperature. Lines represent a linear fit with slopes of $-6 \times 10^{-4}$/K and −0.064%/K, respectively.

The 10 J amplifier architecture is based on the multislab approach. The gain medium is composed of four circular Yb:YAG slabs with two different Yb doping levels as 1.1 and 2.0 at % to confirm a uniform temperature distribution among each slab. The diameter of the circular slab is 45 mm with a 5 mm thickness, and the pump area is square of 23 × 23 mm$^2$. The pump beam is supplied from 939 nm diodes in stack with a pumping time duration of 700 μs at 10 Hz. The Yb:YAG circular slab is cladded with a 5 mm wide Cr:YAG absorber with 6 cm$^{-1}$ absorption coefficient. This is effective to prevent amplified spontaneous emission (ASE) and parasitic oscillations. A cryogenic He flow cools the slab and keeps the temperature as 150–170 K. The pressure of the He flow is 10 bar. **Figure 17** shows the optical arrangement for amplification. A seed beam is injected into the amplifier through a dichroic mirror and then image relayed by a spatial filter ($f$ = 1 m) to a back reflector and reflected back to the amplifier module. One spatial filter locates on each side of the amplifier head. Each pass is composed by a set of separate mirrors. A deformable mirror is placed in the amplifier after the third pass for the aberration compensation. After seven passes, the beam is extracted from the amplifier with pulse energy increased to 9 J with a size of 21 mm × 21 mm$^2$.

http://dx.doi.org/10.5772/64147

Numerical modeling of the multislab amplifier is conducted in the HiLASE project to ensure the scaling of the cryogenic technology for further increased parameter region in pulse energy, repetition rate, and better beam quality. Comsol Multiphysics software was chosen to model the thermal and stress effects in the amplifiers [43]. The sources of heat were calculated in the ASE code [44]. The axial surfaces of the slabs are assumed to be cooled only by flowing helium gas at 160 K. The slab was assumed to have no thermal contact with its 2 cm thick Invar holder; and all heat is removed by convection through the faces. From the temperature and stress maps of the slab, the optical path difference (OPD) and birefringence depolarization losses were calculated for a single slab according to a prior approach. The gradual decrease of cooling efficiency in the direction of gas flow, caused by He heating, results in the loss of left-right symmetry of the temperature, stress, depolarization, and OPD maps.

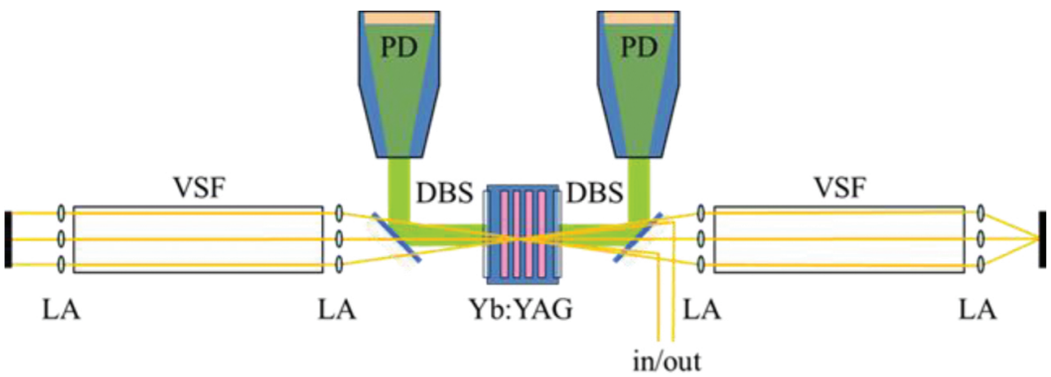


**Figure 17.** Schematic of the 10 J cryogenic multislab amplifier. It consists of Yb:YAG ceramic slabs in the laser head, dichroic beam splitters (DBSs), lens arrays (LAs), vacuum spatial filters (VSFs), and homogenized pump diode laser modules (PDs).

It is planned to increase the repetition rate of the 10 J amplifier to 100 Hz by keeping the basic performance. Once the operation is as expected, the cryogenic laser offers a technological stage for a single module to generate picosecond multipulses of a few joules of energies, for a single-shot imaging Compton source.

## 5. Conclusion

Recent progress of thin-disc lasers is promising to realize a high-brightness pumping source of laser plasma or laser Compton short-wavelength sources. Further progress is possible by an advanced cryogenic technology with its higher thermal conductivity. These laser progresses are contributing in the practical applications in short-wavelength imaging and material processing. Picosecond thin-disc laser technology is now in the stage of 1 kW level with >100 kHz repetition rate. Further research and developments are aiming at 1 kW with kHz repetition rate (1 J, ps, kHz), pulse length reduction into subpicosecond region with MHz repetition rate (mJ, fs, MHz), and increase in the average power to 10 kW region. These challenges require further improvements of the achieved technology bases and evaluation of new schemes.

Cryogenic technology is now offering an option for these challenges in the solid-state laser technology.

## Acknowledgements

The author appreciates kind collaboration of many researchers in HiLASE Centre in Czech Republic, Waseda University, and Gigaphoton Inc., in Japan. Dr. M. Smrz is especially acknowledged for his excellent work in the 100 kHz thin-disc picosecond laser, Dr. H. Turcicova and Dr. O.Novak for their high average power wavelength conversion, and Dr. P. Sikocinski for his aberration measurement in cryogenic Yb:YAG. Dr. Sakaue is highly appreciated for his experimental and theoretical work in the Laser Compton and FEL seeding research and Dr. T. Yanagida for his pioneering work of tin droplet atomization by a picosecond laser. Experimental work of this chapter is cofinanced by the state budget of the Czech Republic (project HiLASE: Superlasers for real world: LO1602). This work is also supported by the Czech Science Foundation (GACR) under project GA16-12960S.

## Author details

Akira Endo

Address all correspondence to: endo@fzu.cz

1 Research Institute for Science and Engineering, Waseda University, Tokyo, Japan

2 HiLASE Centre, Institute of Physics AS CR, Dolní Břežany, Czech Republic

## References

[1] Assoufid, L. and Naulleau, P. (2016) Topical Meeting, Compact (EUV & X-ray) Light Sources, OSA High-Brightness Sources and Light-Driven Interactions Congress, 20–22 March 2016, Hilton Long Beach, Long Beach, California, USA

[2] Mizoguchi, H. Nakarai, H. Abe, T. Nowak, K.M. Kawasuji, Y. Tanaka, H. Watanabe, Y. Hori, T. Kodama, T. Shiraishi, Y. Yanagida, T. Soumagne, G. Yamada, T. Yamazaki, T. Okazaki, S. and Saitou, T. (2015) "Performance of one hundred watt HVM LPP-EUV source," Proceedings of SPIE 9422-11

[3] Reagan, B.A. Berrill, M. Wernsing, K.A. Baumgarten, C. Woolston, M. and Rocca, J.J. (2014) "High-average-power, 100-Hz-repetition-rate, tabletop soft-X-ray lasers at sub-15-nm wavelengths," Phys. Rev. A 89, 053820

[4] John, R.W (1998) "Brilliance of X rays and gamma rays produced by Compton back scattering of laser light from high energy-electrons," Laser Particle Beams 16, 115–127

[5] Endo, A. Yang, J. Okada, Y. Yanagida, T. Yorozu, M. and Sakai, F. (2001) "Characterization of the monochromatic laser Compton X-ray beam with picosecond and femtosecond pulse widths," Proceedings SPIE 4502, pp. 100–108

[6] Babzien, M. Ben-Zvi, I. Kusche, K. Pavlishin, I.V. Pogorelsky, I.V. Siddons, D.P. and Yakimenko, V. (2006) "Observation of the second harmonic in Thomson scattering from relativistic electrons," Phys. Rev. Lett. 96, 054802

[7] Kumita, T. Kamiya, Y. Babzien, M. Ben-Zvi, I. Kusche, K. Pavlishin, I.V. Pogorelsky, I.V. Siddons, D.P. Yakimenko, V. Hirose, T. Omori, T. Urakawa, J. Yokoya, K. Cline, D. and Zhou, F (2008) "Observation of the nonlinear effect in relativistic Thomson scattering of electron and laser beams," Laser Phys. 16, 267–271

[8] Oliva, P. Carpinelli, M. Golosio, B. Delogu, P. Endrizzi, M. Park, J. Pogorelsky, I. Yakimenko, V. Williams, O. and Rosenzweig, J (2010) "Quantitative evaluation of single-shot inline phase contrast imaging using an inverse Compton x-ray source," Appl. Phys. Lett. 97, 134104

[9] Pogorelsky, I.V. Babzien, M. Pavlishin, I. Stolyarov, P. Yakimenko, V. Shkolnikov, P. Pukhov, A. Zhidkov, A. and Platonenko, V.T. (2006) "Terwatt CO2 laser; a new tool for strong field research," Proceedings of SPIE, 6261, 18

[10] Ur.C.A. Balabanski, D. Cata-Danil, G. Gales, S. Morjan, I. Tesileanu, O. Ursescu, D. Ursu, I. and Zamfir, N.V. (2015) "The ELI–NP facility for nuclear physics," Nucl. Instrum. Method B 355, 198–202

[11] Bacci, A. Palmer, D. Serafini, L. Torri, V. Petrillo, V. Tomassini, P. Puppin, E. Alesini, D. Anania, M. Bellaveglia, M.P. Bisesto, F. Pirro, G.Di. Esposito, A. Ferrario, M. Gallo, A. Gatti, G. Ghigo, A. Spataro, B. Vaccarezza, C. VillaF. Cianchi, A. Agostino, R.G. Borgese, G. Ghedini, M. Martire, F. Pace, C. Levato, T. Dauria, G. Fabris, A. and Marazzi, M. (2014) "The STAR Project," Proceedings of IPAC2014, WEPRO115A

[12] Endo, A. Sakaue, K. Washio and M. Mizoguchi, H. (2014) "Optimization of high average power FEL for EUV lithography application," Proceedings of FEL2014, FRA04

[13] Allaria, E. Castronovo, D. Cinquegrana, P. Craievich, P. Dal Forno, M. Danailov, M.B. D'Auria, G. Demidovich, A. De Ninno, G. Di Mitri, S. Diviacco, B. Fawley, W.M. Ferianis, M. Ferrari, E. Froehlich, L. Gaio, G. Gauthier, D. Giannessi, L. Ivanov, R. Mahieu, B. Mahne, N. Nikolov, I. Parmigiani, F. Penco, G Raimondi, L. Scafuri, C. Serpico, C. Sigalotti, P. Spampinati, S. Spezzani, C. Svandrlik, M. Svetina, C. Trovo, M. Veronese, M. Zangrando, D. and Zangrando, M. (2013) "Two-stage seeded soft-X-ray free-electron laser," Nature Photon. 7, 913–918

[14] Höppner, H. Hage, A. Tanikawa, T. Schulz, M. Riedel, R.Teubner, U. Prandolini, MJ. Faatz, B. and Tavella, F. (2015) "An optical parametric chirped-pulse amplifier for seeding high repetition rate free-electron lasers," New J. Phys. 17, 053020

[15] Klenke, A. Breitkopf, Kienel, S.M. Gottscha, T. Eidam, T. Hädrich, S. Rothhardt, J. Limpert, J. and Tünnermann, A. (2013) "530 W, 1.3 mJ, four-channel coherently combined femtosecond fiber chirped-pulse amplification system," Opt. Lett. 38, 2283–2285

[16] Brocklesby, W.S. Nilsson, J. Schreiber, T. Limpert, J. Brignon, A. Bourderionnet, J. Lombard, L. Michau, V. Hanna, M. Zaouter, Y. Tajima, T. and Mourou, G. (2014) "ICAN as a new laser paradigm for high energy, high average power femtosecond pulses," Eur. Phys. J. Special Topics 223, 1189–1195

[17] Mans, T.R. Graf, R. Dolkemeyer, J. Schnitzler, C (2014) "Femtosecond Innoslab amplifier with 300 W average power and pulse energies in the mJ regime," Proceedings of SPIE 8959-43

[18] Negel, J.P. Loescher, A. Voss, A. Bauer, D. Sutter, D. Killi, A. Ahmed, M.A. and Graf.T, (2015) "Ultrafast thin-disk multipass laser amplifier delivering 1.4 kW (4.7 mJ, 1030 nm) average power converted to 820 W at 515 nm and 234 W at 343 nm," Opt. Exp. 23, 21064

[19] Freitag, C. Wiedenmann, M. Negel, J.P. Loescher, A. Onuseit, V. Weber, R. Ahmed, M.A. Thomas Graf, T. (2015)" High-quality processing of CFRP with a 1.1-kW picosecond laser," Appl. Phys. A 119, 1237–1243

[20] Ripin, D.J. Ochoa, J.R. Aggarwal, R.L. Fan, T.Y. (2005) "300-W Cryogenically Cooled Yb:YAG Laser," IEEE J. Quantum Electron, QE-41, 1274–1277

[21] Zapata, L.E. Reichert, F. Hemmer, M. Kaertner, F.X. (2016) "250 W average power, 100 kHz repetition rate cryogenic Yb:YAG amplifier for OPCPA pumping," Opt. Lett. 41, 492–495

[22] Endo, A. Lithography, Chapter 9 (2010) "$CO_2$ laser produced Tin plasma light source as the solution for EUV lithography," edited by Michael Wang, InTech, Janeza Trdine 9, 51000 Rijeka, Croatia

[23] Pirati, A. Peeters, R. Smith, D.A. Lok, S. Noordenburg, M. Es, R. Verhoeven, E. Meijer, H. Minnaert, A. Horst, W. Meiling, H. Mallmann, J. Wagner, C. Stoeldraijer, J. Fisser, G. Levasier, L. Finders, J. Zoldesi, C. Stamm, U. Boom, H. Brandt, D.C. Brown, D.J. and Fomenkov, I.V. (2016) "EUV lithography performance for manufacturing: status and outlook," Proceedings of SPIE 9776-10

[24] Teramoto, Y. Santos, B. Mertens, G. Kops, R. Kops, M. Wezyk, A. Bergmann, K. Yabuta, H. Nagano, A. Ashizawa, N. Shirai, T. Nakamura, K. and Kasama, K. (2016) "High-radiance LDP source: Clean, reliable, and stable EUV source for mask inspection," Proceedings of SPIE 9776-22

[25] Mizoguchi, H. Saitou, T. Yamazaki, T. Okazaki, S. Nakarai, H. Abe, T. Kodama, T. Yanagida, T. Hori, T. Nowak, K.M. Kawasuji, Y. Tanaka, H. Shiraishi, Y. Watanabe, Y.

Yamada, T. and Soumagne, G. (2014) "Sub-hundred Watt operation demonstration of HVM LPP-EUV source," Proceedings of SPIE 9048-22

[26] Smrž, M. Miura, T. Chyla, M. Muzik, J. Nagisetty, S.S. Novák, O. Turcicova, H. Linnemann, Huynh, J. Severová, P. Sikocinski, P. Endo, A. and Mocek, T. (2016) "Progress in kW-class picosecond thin-disk lasers development at the HiLASE," Proceedings of SPIE 9726-43

[27] Smrž, M. Miura, T. Chyla, M. Nagisetty, S. Novák, O. Endo, A. and Mocek, T. (2014) "Suppression of nonlinear phonon relaxation in Yb:YAG thin disk via zero phonon line pumping," Opt. Lett. 39, 4919–4922

[28] Schneidmiller, E.A. , Vogel, V.F. Weise, H. and Yurkov, M.V. (2011) "A kilowatt-scale free electron laser driven by L-band superconducting linear accelerator operating in a burst mode," International Workshop on EUV and Soft X-ray Sources, November 7–9, 2011, Dublin, Ireland

[29] Hosler, E.R. Wood, O.R. Barletta, W.A. Mangat, P.J., Preil, M.E. (2015) "Considerations for a free-electron laser-based extreme-ultraviolet lithography program," Proceedings of SPIE, 9422-12

[30] Chalupský, J. Juha, L. et.al. (2007) "Characteristics of focused soft X-ray free-electron laser beam determined by ablation of organic molecular solids," Opt. Exp. 15, 6036

[31] Filippetto D. Byrd, J. Chin, M. Cork, C. Santis, S.De. Feng, J. Norum, W.E. Doolittle, L. Papadopoulos, C. Portmann, G. Quintas, D.G. Sannibale, F. Stuart, M. Wells, R. and Zolotorev, M. (2011) "Low energy beam diagnostic for APEX, the LBNL VHF photoinjector," Proceedings of 2011 Particle Accelerator Conference, WEP222

[32] Nakajyo, T. Yang, J. Sakai, F. and Aoki, Y. (2003) "Quantum efficiencies of Mg photocathode under illumination with 3rd and 4th harmonics Nd: LiYF4 laser light in RF gun," Jpn. J. Appl. Phys. 42 1470–1474

[33] Singer, A. Sorgenfrei, F. Mancuso, A.P. Gerasimova, N. Yefanov, O.M. Gulden, J. Gorniak, T. Senkbeil, T. Sakdinawat, A. Liu, Y. Attwood, D. Dziarzhytski, S. Mai, D.D. Treusch, R. Weckert, E. Salditt, T. Rosenhahn, A. Wurth, W. and Vartanyants, A. (2012) "Spatial and temporal coherence properties of single free electron laser pulses," Opt. Exp. 20, 17480

[34] Turcicova, H. Nowak, O. Smrz, M. Miura, T. Endo, A. and Mochek, T. "Deep ultraviolet (257.5 nm and 206 nm) picosecond pulses produced a high-power 100 kHz solid-state thin-disk laser," Proceedings of SPIE 9893-1

[35] Riedel, R. Rothhardt, J. Beil.K, Gronloh, B. Klenke, A. Höppner, H. Schulz, M., Teubner, Kränkel, U.C. J.Limpert, J. Tünnermann, A. Prandolini, M.J. F. and Tavella, F. (2014) "Thermal properties of borate crystals for high power optical parametric chirped-pulse amplification," Opt. Exp. 22, 17607.

[36] Stubenvoll, M. Schäfer, B. Mann, K. and Novak, O. (2016) "Photothermal method for absorption measurements in anisotropic crystals," Rev. Sci. Instrum. 87, 023904, Proceedings of SPIE 9726-43

[37] Sakaue, K. Araki, S. Fukuda, M. Higashi, Y. Honda, Y. Sasao, N. Shimizu, H. Taniguchi, T. Urakawa, J. and Washio, M. (2011) "Development of a laser pulse storage technique in an optical super-cavity for a compact X-ray source based on laser-Compton scattering," Nucl. Instru. Meth. A 637, S107–S111

[38] Courjaud, A. Tropheme, B. Falcoz, F. Eric, P. Mottay, E.P. and Riboulet, G. (2015) "High power lasers for gamma source," Proceedings of SPIE 9342-23

[39] Jung, R. Tümmler, J. Nubbemeyer, T. and Will, I. (2015) "Two- Channel thin-disk laser for high pulse energy," Advanced Solid State Lasers Conference© OSA 2015, AW3A.7.

[40] Fan, T.Y. Ripin, D.J. Aggarwal, R.L. Ochoa, J.R. Chann, B. Tilleman, M. and Spitzberg, J. (2007) "Cryogenic Yb3+-Doped Solid-State Lasers," IEEE J. Quantum Electron. QE-13, 448–458

[41] Sikocinski, P. Novak, O. Smrz, M. Pilar, J. Jambunathan, V. Jelínková, H. Endo, A. Lucianetti, A. and Mocek, T. (2016) "Time-resolved measurement of thermally induced aberrations in a cryogenically cooled Yb:YAG slab with a wavefront sensor," Appl.Phys.B. April 2016, 122:73

[42] Mason, P.D. Banerjeea, S. Ertela, K. Phillipsa, P.J. Thomas, J. Butchera, T.J. Smitha, J.M. Vidoa, M.D. Tomlinsona, S. Oleg Chekhlova, O. Shaikha, W. Blakea, S. Holligana, P. Divoky, M. Pilar, J Hernandez-Gomeza, C. Justin, R. Greenhalgha, S. and Colliera, J.L. (2015) "DiPOLE100: A 100 J, 10 Hz DPSSL using cryogenic gas cooled Yb:YAG multi slab amplifier technology," Proceedings of SPIE 9513 02-1

[43] Slezak, O. Lucianetti, A. Divoky, M. Sawicka, M. and Mocek, T. (2013) "Optimization of wavefront distortions and thermal-stress induced birefringence in a cryogenically-cooled multislab laser amplifier," IEEE J. Quantum Electron, QE 49, 960–966

[44] Sawicka, M. Divoky, M. Novak, J. Lucianetti, A. Rus, B. and Mocek, T. (2012) "Modeling of amplified spontaneous emission, heat deposition, and energy extraction in cryogenically cooled multislab Yb3+:YAG laser amplifier for the HiLASE Project," J. Opt. Soc. Am. B 29, 1270–1276